High figure-of-merit in Al-doped ZnO thin films grown by ALD through the Al content adjustment

Quang Chieu Bui, Vincent Consonni, Sarah Boubenia, Guillaume Gay, Corinne Perret, Mohammed Zeghouane, Sebastien Labau, Hervé Roussel, Xavier Mescot, Gustavo Ardila, et al.

High Figure-of-Merit in Al-Doped ZnO Thin Films Grown by ALD through the Al Content Adjustment

Quang Chieu Bui,[a,b,c] Vincent Consonni,[b*] Sarah Boubenia,[a] Guillaume Gay,[a] Corinne Perret,[a] Mohammed Zeghouane,[a] Sebastien Labau,[a] Hervé Roussel,[b] Xavier Mescot,[c] Gustavo Ardila,[c] and Bassem Salem.[a*]

[a] *Univ. Grenoble Alpes, CNRS, CEA/ LETI Minatec, Grenoble INP, LTM, F-38054 Grenoble, France.*

[b] *Univ. Grenoble Alpes, CNRS, Grenoble INP, LMGP, F-38000 Grenoble, France.*

[c] *Univ. Grenoble Alpes, CNRS, Grenoble INP, IMEP-LAHC, F-38000 Grenoble, France.*

*Corresponding authors: vincent.consonni@grenoble-inp.fr and bassem.salem@cea.fr

ABSTRACT

The development of transparent conductive materials is of great interest for a wide variety of semiconducting devices in the fields of optoelectronics and photovoltaics. Here, we optimize the growth and properties of aluminum-doped ZnO (AZO) thin films as an eco-friendly transparent electrode by using atomic layer deposition (ALD) with diethylzinc (DEZn), water vapor and trimethylaluminium (TMA) as zinc, oxygen, and aluminium chemical precursors, respectively. The cycle ratio of DEZn to TMA using ALD is adjusted to control the Al atomic concentration over a broad range of 0.3 - 6.7% while optimizing the structural, optical, and electrical properties of AZO thin films. By incorporating a sufficient amount of Al dopants around 1.1%, we obtained a high quality AZO thin film exhibiting a low electrical resistivity of 6.3×10^{-4} Ω·cm. This AZO thin film grown on quartz substrate also demonstrates an average optical transmittance in the visible range above 85% as well as a high figure-of-merit of 6.4×10^{-3} Ω^{-1}, while maintaining its highly *c*-axis oriented structure. The present optical and electrical properties result in the fabrication of AZO thin films by ALD with a high figure-of-merit that is highly suitable for many semiconducting devices.

KEYWORDS: ZnO, AZO, Atomic Layer Deposition, Nanostructures, Transparent conductive oxide.

1. Introduction

Indium tin oxide (ITO) is considered as the most common transparent conductive material (TCM) and is used as transparent electrode for many applications thanks to its low electrical resistivity (< 10^{-4} Ω·cm) and its high visible light transmittance (> 85%) [1,2]. However, indium is a critical element owing to its scarcity and its compound is toxic [2–4], requiring the development of alternative TCMs. Besides ITO, aluminum-doped zinc oxide (AZO) [5], fluorine-doped zinc oxide (FZO) [6], fluorine-doped tin oxide (FTO) [7], silver nanowires [8], and graphene [9], to name a few, have thus received an increasing interest over the past decade. Among them, AZO is an attractive TCM to replace ITO as it is not only composed of low-cost abundant elements, non-toxic, but also has a low electrical resistivity and high optical transmittance [2]. For instance, B. Sarma *et al.* showed the fabrication of a 341 nm-thick AZO thin film deposited by pulsed DC magnetron sputtering with the electrical resistivity as low as 3.07 x 10^{-4} Ω·cm and the visible light transmittance higher than 80 % [5]. The AZO thin film has therefore been developed for different applications such as transistors [10], solar cells [11], organic light-emitting devices (OLED) [12], gas sensors [13], and piezoelectric nanogenerators [14]. In particular, the AZO thin film is a promising transparent electrode for developing nanostructure-based devices including eco-friendly ZnO-based piezoelectric devices. Beside the low electrical resistivity and high visible light transmittance, the structural properties of the AZO thin film also play an important role when it is integrated as a bottom transparent electrode into a nanostructure-based device. As the AZO thin film is used as a growth platform in the process flow of some of the semiconductor-based technology, its surface morphology and structural orientation can significantly affect the deposition of a material that has an epitaxial relationship as well as the resulting performance of the device. For instance, S. Pung *et al.* demonstrated that the growth direction of ZnO NWs was dependent upon the orientation of the ZnO thin film used as a growth platform [15]. Thus, it is very important to control both the structural and electrical properties of AZO thin films acting as transparent electrodes during its fabrication process when integrated into a number of nanostructure-based devices.

AZO thin films can be grown by magnetron sputtering [5], pulsed-laser deposition (PLD) [16], sol-gel process [17], metal-organic chemical vapor deposition (MOCVD) [18], and atomic layer deposition (ALD) [12]. Among these deposition techniques, the ALD process exhibits a number of assets including the compatibility with a large surface area and the formation of deposits with a high uniformity and precisely controlled thickness. While this technique has a very low growth rate due to the self-limited process on the surface, it is also able to produce a high uniformity and smooth surface thin film over a high aspect ratio structure, making it highly relevant in the process flow of nanostructure-based devices. AZO thin films have been grown by ALD using different process parameters, such as the growth temperature [19] and Al doping concentration [19,20], and on different substrates [21]. The AZO thin films grown by ALD can achieve a relatively low electrical resistivity

that is still higher than the electrical resistivity of AZO thin films grown by magnetron sputtering or of ITO thin films, while exhibit a high visible light transmittance as reported by J. Kim *et al.* [22].

In this work, the structural orientation of AZO thin films is tuned while maintaining its low electrical resistivity and high visible light transmittance by adjusting the Al doping concentration during the ALD process. The Al content in the AZO thin films is investigated by parallel angular X-ray photoelectron spectroscopy (XPS) while a large variation of their morphology and structural orientation is studied by field-emission scanning electron microscopy (FESEM) and X-ray diffraction (XRD). The electrical properties of AZO thin films are measured by the Hall-effect method, and their optical transmittance is recorded by UV–Vis-NIR spectrophotometry. The correlation between the structural, electrical, and optical properties of AZO thin films is discussed in detail. A high figure-of-merit (FOM) of 6.4 x 10^{-3} Ω^{-1} is reported while ensuring a high structural quality compatible with nanostructure-based devices.

2. Experiment

2.1 AZO electrodes grown by ALD

The undoped ZnO and AZO thin films were synthesized by ALD in a Cambridge NanoTech Fiji F200 system. Diethylzinc (DEZn), trimethyl aluminum (TMA) and water vapor (DI) were used as the Zn, Al and O precursors, respectively. The thin films were formed following the succession of many super cycles. For the AZO thin films, a super cycle consisted of *n* cycles for ZnO deposition and 1 cycle for Al_2O_3 deposition. The super cycle started with n/2 pulses of DEZn, following by a pulse of TMA, and then finished with n/2 pulses of DEZn. The pulse durations of DEZn and TMA were set at 0.015 seconds. The *n* value was varied at 40, 30, 20, and 10 to form the AZO thin films with different Al doping concentrations, which are denoted as the AZO40, AZO30, AZO20, and AZO10 samples, respectively. The undoped ZnO was grown by removing the cycle for Al_2O_3 deposition from the super cycle. The total number of cycles were kept at around 1320 for every growth to obtain the same thickness (~180 nm). The substrate temperature was set to 250 °C. The growths were performed simultaneously on standard Si (100) with an electrical resistivity of around 10 Ω·cm and on quartz.

2.2 Characterizations

FESEM images of undoped ZnO and AZO thin films were collected using a ZEISS Gemini 300 SEM instrument. To study the chemical composition of undoped ZnO and AZO thin films, XPS analyses were performed on a customized Thermo Fisher Scientific Theta 300 system with ultrahigh vacuum conditions (< 1×10^{-8} Pa) equipped with an X-ray source using a monochromatic aluminum anode (1486.6 eV). The ejected electrons were collected by a hemispherical analyzer at 100 eV constant pass energy. The energy scale was calibrated using the surface C 1s peak, from the carbon contamination, at 284.8 eV. The root mean square (RMS) roughness of thin films was evaluated using

a BRUKER Dimension Icon atomic force microscope (AFM). Their XRD patterns were recorded with a BRUKER D8 Advance diffractometer using Cu $K\alpha_1$ radiation according to the Bragg–Brentano configuration, using a 2θ-scale range of 20 − 140°. The optical transmittance of undoped ZnO and AZO thin films deposited on quartz was measured with a PERKIN-ELMER Lambda 950 UV–Vis-NIR spectrophotometer equipped with an integrating sphere. The electrical resistivity, charge carrier density and mobility of thin films were investigated by Van der Pauw and Hall-effect measurement method using a home-made station. To quantitatively evaluate and compare the performance of TCMs, a figure-of-merit (FOM) has usually been used as a numerical value involving the visible light transmittance and the electrical resistivity, which are the two most important optical and electrical properties for transparent electrodes. Here, the FOM values (Φ_{TC}) of AZO thin films were calculated as follows [5,23,24]:

$$\Phi_{TC} = \frac{T^{10}}{R_{Sh}} \quad (1)$$

where T is the mean optical transmittance determined in the light wavelength range of 400 − 700 nm, and R_{Sh} is the sheet resistance of thin films.

3. Results and discussion

3.1. Morphology of undoped ZnO and AZO thin films

The FESEM images of undoped ZnO and AZO thin films grown by ALD with different Al doping concentrations are presented in **Figure 1**. By maintaining the total number of cycles at around 1320 for every ALD process, the thickness of thin films is kept similar at around 180 nm, as shown in the cross-sectional-view FESEM images. However, the morphologies presented in the top-view FESEM images differ, indicating its dependence on the Al doping concentration. The undoped ZnO thin film presents big irregular shape grains along with other smaller round grains. The small round shape grains and elongated grains observed specifically on the AZO30 and AZO20 thin films are related to the (002) and (100) planes of the wurtzite structure of ZnO, respectively, as reported in refs.[19,25,26]. Correspondingly, the RMS roughness measured by AFM on the undoped ZnO thin film shows the highest value at 2.8 nm. The RMS roughness decreases to 2.3 nm on the AZO40 thin film, and to around 1.3 nm on the other samples.

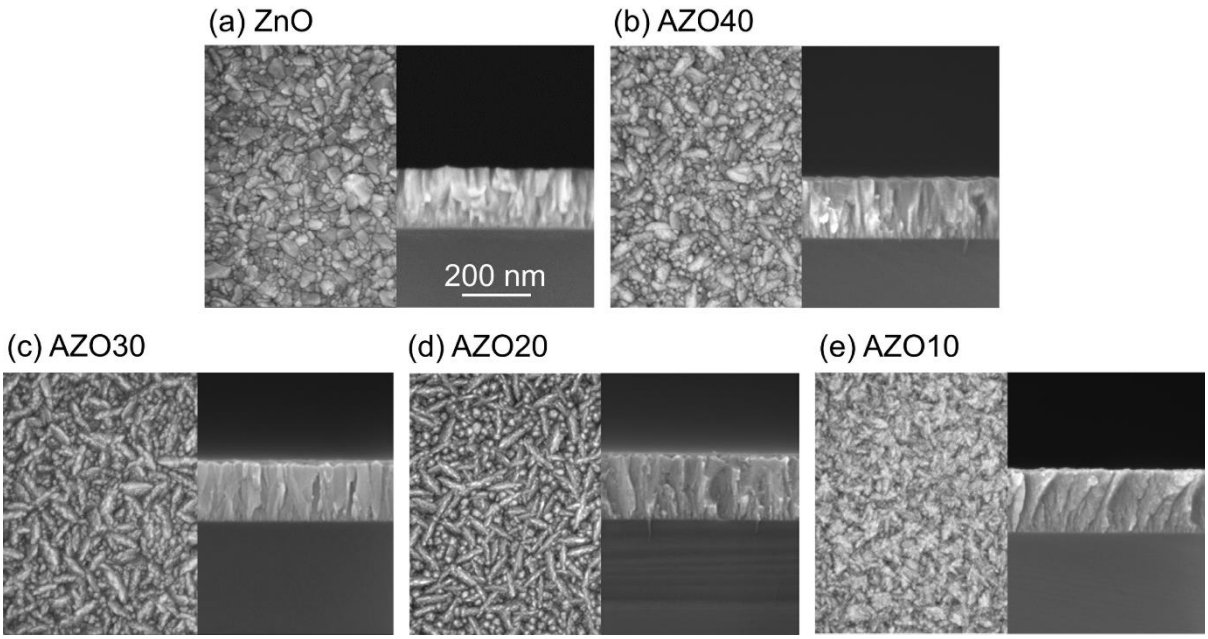

Figure 1: Top-view (left) and cross-sectional-view (right) FESEM images of undoped ZnO and AZO thin films grown by ALD with different Al doping concentrations.

3.2 Al content in undoped ZnO and AZO thin films

XPS measurements were performed to evaluate the content of Al atoms incorporated into AZO thin films, as presented in **Figure 2**. For each sample, the angle between the focus beam and sample surface was varied from 23.75 to 76.25° in order to analyze the chemical composition from the surface down to a depth of 5 nm of the AZO thin films. The data was collected at all angles simultaneously by parallel angular XPS measurements. The Al 2p core level, acquired in-depth at 23.75°, is located around 74 eV in the XPS spectra of AZO thin films and, as expected, it is not detected in the XPS spectrum of undoped ZnO thin film, as shown in **Figure 2a**. The intensity of the Al-related peak decreases as the Zn/Al-precursor cycle ratio is increased. The average values of Al atomic concentration measured at different angles were calculated and shown in **Figure 2b**. The data indicates that the Al atoms are incorporated into AZO thin films, and that their atomic concentration increases from 0.3 to 6.7% as the Zn/Al-precursor cycle ratio is decreased from 40 to 10.

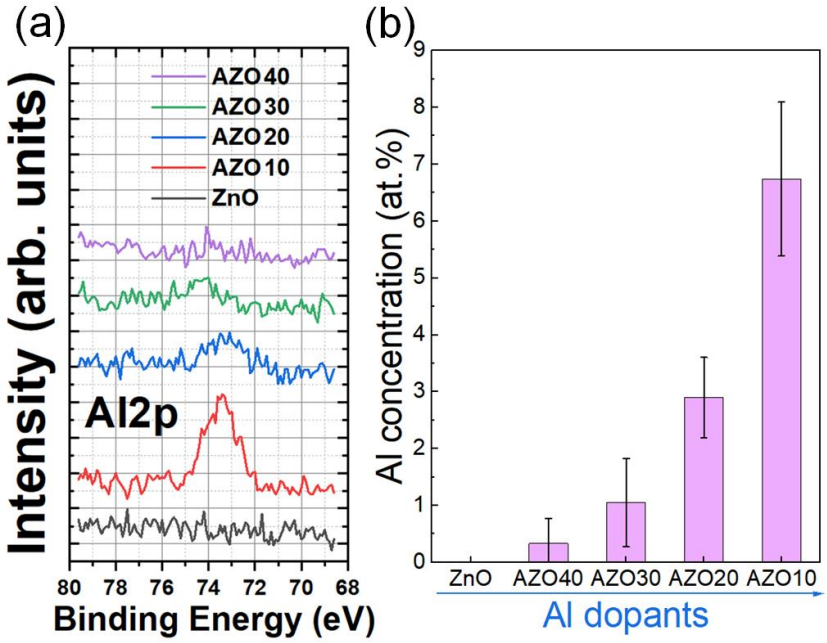

Figure 2: (a) XPS spectra and (b) concentration of Al atoms inside undoped ZnO and AZO thin films grown by ALD with different Al doping concentrations. The values of Al atomic concentration were averaged at different angles between the focus beam and the sample surface during the XPS acquisition.

3.3 Growth texture and strain of undoped ZnO and AZO thin films

Figure 3 shows the XRD patterns of undoped ZnO and AZO thin films grown by ALD with different Al doping concentrations. The 100, 002, 101, 102, 103, and 004 diffraction peaks corresponding to the wurtzite structure of ZnO are located at 31.8, 34.4, 36.3, 47.5, 62.9, and 72.6°, as indicated by the International Center for Diffraction Data (ICDD) file labelled 00-036-1451. Besides the peaks of Si and ZnO, no other diffraction peaks coming from any Al-related compound are detected, showing that Al atom only acts as a dopant inside AZO thin films. The XRD pattern of undoped ZnO thin film exhibit many diffraction peaks with similar intensities, expressing a random orientation in this thin film as seen in **Figure 3a**. This differs from the ZnO thin films grown by MOCVD as shown in ref. [27], in which the structure is highly oriented along the *c*-axis as indicated by the high intensity of the 002 diffraction peak as compared to other peaks. Normally, the growth texture is expected to follow the evolutionary selection model given by van der Drift, where the grains with the fastest growth direction develop at the expenses of the others and hence dominate the overall orientation [28]. Here, the ZnO growth direction is the fastest one along the *c*-axis since the polar *c*-planes exhibit the highest surface energy in the wurtzite structure [29]. The suppression of the growth texture along the *c*-axis during ALD process was also reported in ref. [15] and attributed to the interference of organic molecules dissociated from the DEZn precursor. Particularly, the negatively charged CH_3CH_2- group can attach to the positively charged Zn-polar surface, inhibiting the

development on this plane. Due to the limited reactive sites during the ALD process, the Zn and O adatoms move to other reactive sites on other planes. In addition, the present ZnO growth by ALD was performed on Si substrate, which has no epitaxial relationship with ZnO, and the growth temperature in ALD chamber (250 °C) is much lower as compared to a typical MOCVD chamber (500 – 700 °C) [27], leading to a much lower diffusion length of adatoms. All of these phenomena cause the ZnO thin films to develop along several growth directions and hence to exhibit an overall random orientation.

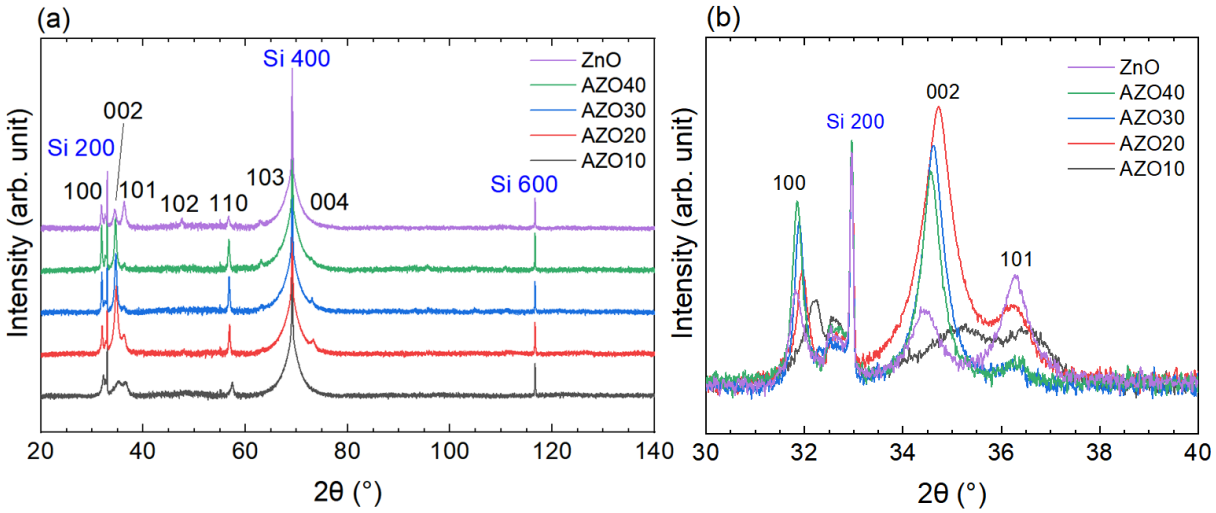

Figure 3: (a) XRD of undoped ZnO and AZO thin films grown by ALD with different Al doping concentrations; (b) Zoom-in in the area of interest ranging from 30 to 40° in the XRD patterns. The intensity was plotted in logarithmic scale.

As long as the TMA precursor was added during the ALD process for the Al doping, the 002, 100 and 110 diffraction peaks become more intense as seen in the AZO40 thin film in **Figure 3b**, demonstrating the preferential growth on the polar *c*-plane, non-polar *m*- and *a*-planes, respectively. By increasing the Al doping concentration in AZO30 and AZO20 thin films, the intensity of the 002 diffraction peak continues increasing, while the intensities of the 100 and 110 diffraction peaks decrease. Simultaneously, the intensities of the 101, 102 and 103 diffraction peaks representing the semi-polar planes are strongly reduced and these peaks end up vanishing. This also corresponds to the predominance of the round and elongated grains and the disappearance of other irregular shape grains in AZO30 and AZO20 thin films, as seen in **Figures 1c-d**. The AZO thin films with a highly *a*-axis oriented structure grown by ALD has been reported in refs.[19,26,30]. The participation of Al^{3+} ions is expected to increase the surface energy of non-polar *m*- and *a*-planes, resulting in a faster growth in these directions. The results in refs.[26,30] have demonstrated that the growth along the *c*-axis is suppressed regardless of the Al doping concentration. In contrast, our results show that the ZnO thin films are grown even faster on the *c*-planes with the increase in the Al doping concentration, as reported in refs.[19,31]. Although the used precursors are the same, there are differences in ALD systems and processes, including the growth temperatures and flow rates used. These factors also

strongly influence the Al incorporation inside ZnO thin films, causing a distortion of ZnO lattice and largely varying the relative surface energies as well as the growth rate of ZnO crystalline planes [19].

In AZO10 thin film, the intensities of the 002 and all other diffraction peaks suddenly decrease while their widths increase, as seen in **Figure 3b**. This indicates that the Al doping concentration is so high that it disrupts the formation of ZnO, resulting in a poor crystalline quality. Combined with the FESEM image in **Figure 1e**, it is deduced that the AZO10 thin film is partially crystallized, which is similar to the observation in ref.[32]. Additionally, the diffraction peaks are also shifted strongly to higher 2θ values when the Al doping concentration is increased. In order to get a more accurate assessment of the structural properties of undoped ZnO and AZO thin films, the texture coefficients of crystallite planes and the homogeneous residual strain as presented in **Figure 4** were calculated based on the intensities and the positions of diffraction peaks using the same method as in our previous works [27,33,34]. The texture coefficients C_{hkl} (in percentage unit) for a given (*hkl*) plane were calculated from the *hkl* diffraction peak as follows:

$$C_{hkl}(\%) = \frac{\frac{I_{hkl}}{I_{0,hkl}} \times 100}{\sum_{i=1}^{N} \frac{I_{h_i k_i l_i}}{I_{0,h_i k_i l_i}}} \qquad (2)$$

where I_{hkl} is the *hkl* peak intensity, $I_{0,hkl}$ is the reference *hkl* peak intensity as given in the 00-036-1451 ICDD file, and N is the number of diffraction peaks considered (here is 6).

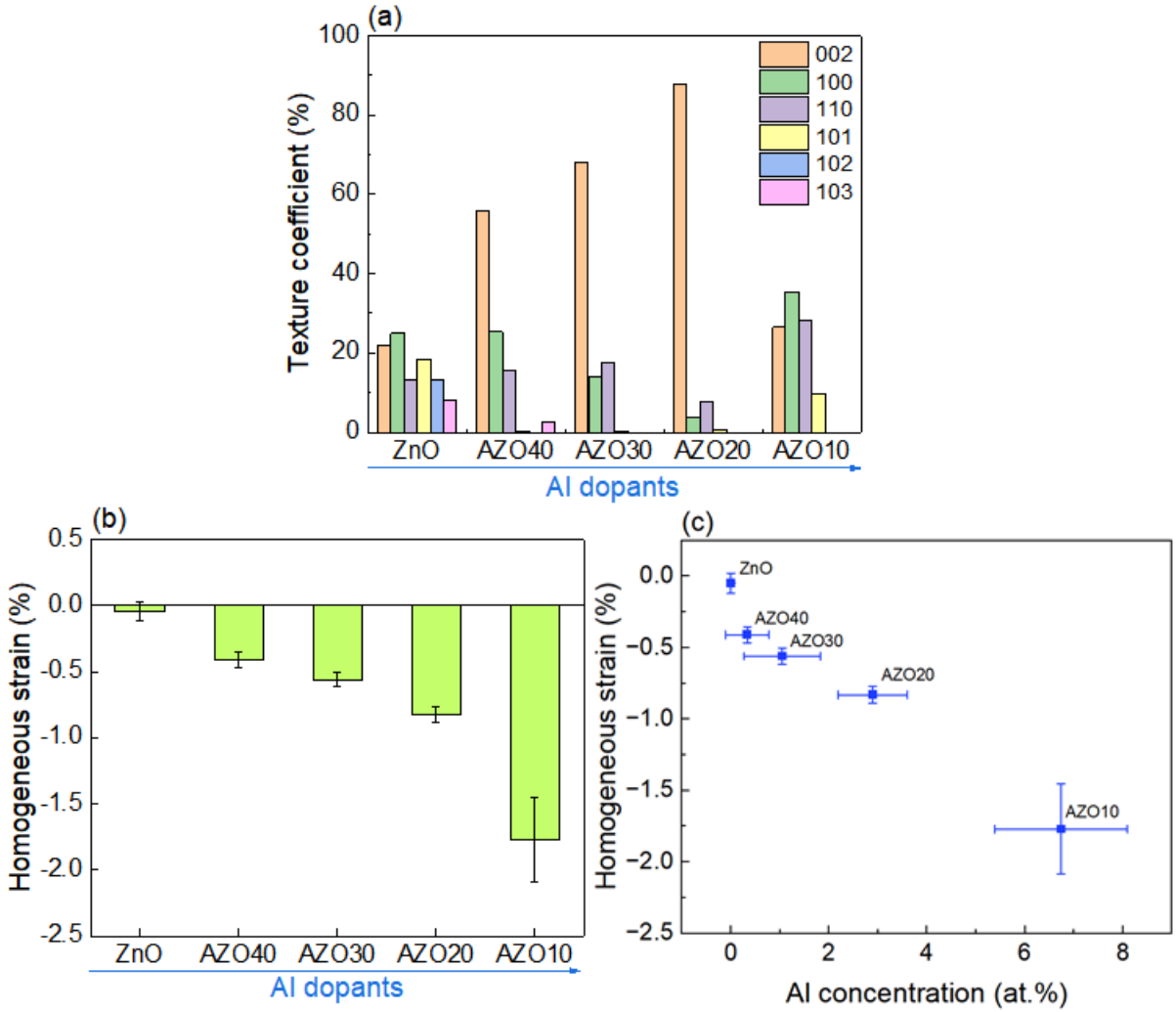

Figure 4: (a) Texture coefficients and (b) mean homogeneous strain of undoped ZnO and AZO thin films grown by ALD with different Al doping concentrations; (c) Evolution of the mean homogeneous strain as measured by XRD as a function of the Al atomic concentration as measured by XPS.

When the Al doping concentration is increased by tuning the Zn/Al-precursor cycle ratio, the (002) texture coefficient continuously increases from 22.0 % in undoped ZnO thin film to 87.8 % in AZO20 thin film, as shown in **Figure 4a**. Simultaneously, the texture coefficients of (101), (102) and (103) semi-polar planes decrease close to 0 when a small amount of the Al dopant is added in the AZO40 thin film. The texture coefficients of (100) non-polar plane starts decreasing when more Al dopants are added in the AZO30 thin film, and the texture coefficients of (110) non-polar plane also decrease in the AZO20 thin film. Further adding Al dopants leads to the formation of partially crystallized AZO10 thin film, for which the 002 texture coefficient drastically decreases to 26.4 % while other plane texture coefficients increase again. In **Figures 4b and c**, the residual strain is found to constantly increase with the Al doping concentration, indicating the incorporation of Al dopants into the ZnO lattice that causes its distortion. In details, **Figure 4b** shows that the ZnO thin film grown by the ALD process has a nearly strain-free state, which is opposite to the ZnO thin film grown by the

MOCVD process [27]. The ZnO thin films grown by MOCVD undergo a significant compressive strain, which is generated during the 3D Volmer-Weber growth mode. In the ALD process, the ZnO thin films are forced to grow in 2D layer-by-layer mode by limiting the number of reactive sites on the substrate surface during each cycle. Thus, the strain is easier to be relaxed when the adatoms are well-arranged on the surface. The negative (compressive) strain appears and increases when the Al dopant is incoporated, indicating that the Zn^{2+} ions are substituted by Al^{3+} ions inside the ZnO lattice. Since the Al^{3+} ion radius (0.53 Å) is smaller than the Zn^{2+} ion radius (0.74 Å), the lattice parameter is reduced when Al^{3+} ions replace Zn^{2+} ions, resulting in the shift of the diffraction peak to higher 2θ values as well as the generation of a compressive biaxial strain [19,20,35]. It can be seen that the strain is increased linearly with the addition of Al content in AZO40, AZO30 and AZO20 thin films (**Figure 4c**), along with the higher preferential growth along the *c*-axis (**Figure 4a**). The residual strain is again rapidly increased to -1.77 % in AZO10 thin film due to a larger amount of Al dopants incorporated into the ZnO lattice, leading to a formation of a partially crystallized thin film. Therefore, an excessive Al doping leads to the degradation of the crystallinity of thin films as revealed in the AZO10 thin film, but a sufficient Al doping concentration helps to improve the *c*-axis orientation as shown in the AZO20 thin film.

3.4 Electrical properties of ZnO and AZO thin films

The electrical resistivity, charge carrier density and mobility of undoped ZnO and AZO thin films grown on standard Si by ALD with different Al doping concentrations are presented in **Figure 5**. The electrical measurements performed on thin films grown on quartz showed similar results. Moreover, we also fabricated metallic electrodes on the sample layer surfaces in order to ensure a good electrical contact between the probes of the measurement station and the thin films. The metallic electrodes were made of 50 nm-thick nickel (Ni) and 120 nm-thick gold (Au) layers, which were deposited on the thin film surfaces using photolithography followed by lift-off processes. The measurements with and without the metallic electrodes gave similar results. In **Figure 5a**, the undoped ZnO thin film shows an electrical resistivity of 7.8 x 10^{-3} Ω·cm, which is notably low owing to the presumable incorporation of hydrogen. Many studies have shown that hydrogen impurities can be generated from the decomposition of DEZn precursor or water vapor during the ALD process, leading to an unintentional hydrogen incorporation in ZnO film [36–38]. These hydrogen dopants can act as shallow donors inside the ZnO structure and decrease its electrical resistivity [37,39]. Following the addition of the TMA precursor during the ALD process, the electrical resistivity further decreases to 6.3 – 7.4 x 10^{-4} Ω·cm in AZO40, AZO30, and AZO20 thin films, revealing the contribution of Al dopants to the electrical conductivity. This is also evidenced in **Figure 5b** by a significant increase in the charge carrier density from 1.6 x 10^{20} cm^{-3} in undoped ZnO thin film to around 2.6 x 10^{21} cm^{-3} in AZO40, AZO30, and AZO20 thin films, demonstrating that the Al dopant acts as a shallow donor inside the ZnO structure. **Figure 5c** shows that the charge carrier mobility decreases from 5.1

cm²/(V·s) in undoped ZnO thin film to around 3.5 cm²/(V·s) in AZO40, AZO30 and AZO20 thin films despite the higher structural quality of AZO films compared to the undoped ZnO film. This could be due to the increase of ionized impurity scattering when the Al dopants are incorporated into the ZnO lattice, causing a decrease of mobility in AZO films [40]. By further doping in AZO10 thin film, the electrical resistivity no longer decreases but instead increases to 5.5 x 10^{-3} **Ω**·cm. This could be due to its partially crystallized structure, where many defects with incomplete atomic bonding can trap and immobilize the charge carriers [41]. The charge carrier mobility and density of AZO10 thin film could not be measured using the Van der Pauw method. It is believed that the mobility in AZO10 thin film is drastically decreased to such a small value that is out of the limit for the measurement station. It is worth mentioning that the AZO30 thin film has the lowest electrical resistivity of 6.3 x 10^{-4} **Ω**·cm, corresponding to the highest electrical conductivity of 1587.6 S/cm as compared to other highly conductive AZO thin films grown by ALD as reported in refs.[12,19,26,30,32,43], as shown in **Figure 5d**. This shows that the AZO30 film is a good candidate to be used as bottom electrode in nanostructure-based devices.

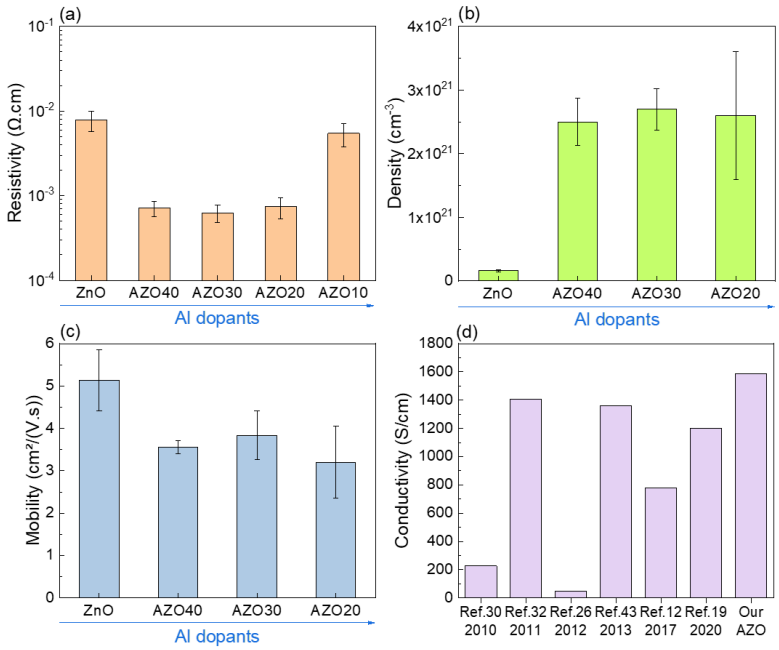

Figure 5: (a) Electrical resistivity, (b) charge carrier density and (c) charge carrier mobility of undoped ZnO and AZO thin films grown on standard Si by ALD with different Al doping concentrations; (d) highest electrical conductivity of AZO thin films grown by ALD in refs.[12,19,26,30,32,43] and in our work.

3.5 Optical transmittance of undoped ZnO and AZO thin films

The optical transmittance spectra in **Figure 6a** show that the undoped ZnO and AZO thin films grown on quartz by ALD with different Al doping concentrations are highly transparent in the visible light region (400 – 700 nm). In this range, the average optical transmittance of these thin films,

including the optical transmittance of quartz, lies in the range of 84 – 87%. At around 650 nm, the optical transmittance reaches a value up to 92 – 93 %, which is close to the optical transmittance of quartz. Excluding the optical transmittance of quartz, the average optical transmittance of undoped ZnO and AZO thin films ranges from 90% to 93%, while their transmittance at 650 nm reaches 98 – 99%. This shows their potential for optical applications. Additionally, it can be noticed in **Figure 6a** that the absorption edge shifts to lower wavelength (higher energy) as the Al doping concentration is increased. To clarify this variation, the optical band gap energies of undoped ZnO and AZO thin films were extracted using Tauc relationship [19]:

$$(\alpha h\nu)^n = A\left(h\nu - E_g\right) \quad (3)$$

where α is the absorption coefficient, $h\nu$ is the photon energy, n is equal to 2 for direct bandgap semiconductors (i.e. ZnO), A is a constant, and E_g is the optical bandgap energy. The absorption coefficient α can be calculated from the optical transmittance as follows [17]:

$$\alpha = \frac{-\ln(T)}{t} \quad (4)$$

where T is the optical transmittance, and t is the thickness of thin films. By plotting $h\nu$ versus $(\alpha h\nu)^2$ within a Tauc plot and fitting the linear part of the curve, E_g can be deduced from the X-intercept of the linear curve. The Tauc plots and the deduced optical band gap energies of undoped ZnO and AZO thin films are presented in **Figures 6b-c**, respectively. The optical band gap energy is found to constantly increase from 3.29 eV in undoped ZnO thin film to 3.91 eV in AZO10 thin film. The increase in the optical band gap energy of AZO thin films as the Al doping concentration is increased can be attributed to the Moss-Burstein effect: the additional Al dopants acting as shallow donors fill the lowest energy states of the conduction band, causing a shift of the Fermi level to the higher energy in the conduction band [5,19,26,30,32].

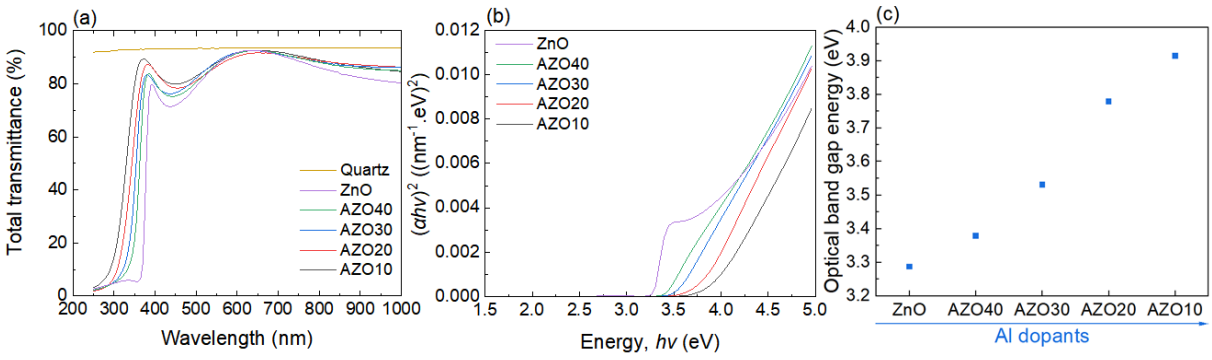

Figure 6: (a) Optical transmittance of undoped ZnO and AZO thin films grown on quartz by ALD with different Al doping concentrations; (b) Tauc plot; (c) optical band gap energy deduced from Tauc plot.

The values of thickness, sheet resistance, mean optical transmittance, and FOM of undoped ZnO and AZO thin films are presented in **Table 1**. A comparison of the visible transmittance and sheet

resistance of our AZO thin films with other AZO and ITO thin films grown by different techniques is shown in **Figure 7**. In this figure, we specifically focus on the comparison of AZO thin films with a thickness below 300 nm. This small thickness is of interest due to its benefits in reducing materials cost and ALD process time. Additionally, limiting the thickness of the films is crucial for electrode integration. Moreover, the optical transmittance values presented in this figure exclude the contribution of the substrates, thus the comparison focuses solely on the transmittance properties of the AZO thin films.

Table 1: Average thickness, sheet resistance, optical transmittance and figure-of-merit values of undoped ZnO and AZO thin films grown by ALD with different Al doping concentrations.

Sample	**Thickness *t* (nm)**	**Sheet resistance R_{Sh} (Ω/square)**	**Mean optical transmittance *T* (%) (including transmittance of quartz)**	**Mean optical transmittance *T* (%) (excluding transmittance of quartz)**	**Figure-of-merit Φ_{TC} (Ω^{-1})***	**Figure-of-merit Φ_{TC} (Ω^{-1})****
ZnO	176	443.8	84.2	90.2	0.41×10^{-3}	0.8×10^{-3}
AZO40	177	40.1	85.4	91.4	5.13×10^{-3}	10.15×10^{-3}
AZO30	181	34.8	86.1	92.1	6.40×10^{-3}	12.66×10^{-3}
AZO20	196	37.8	85.9	92	5.81×10^{-3}	11.48×10^{-3}
AZO10	187	291.4	87.1	93.3	0.86×10^{-3}	1.71×10^{-3}

* Figure-of-merit values are calculated based on the mean optical transmittance including transmittance of quartz.

** Figure-of-merit values are calculated based on the mean optical transmittance excluding transmittance of quartz.

The results show that the FOM values of AZO thin films grown on quartz lie in the range of 0.86 – 6.40 x 10^{-3} Ω^{-1}. Excluding the transmittance of quartz, the FOM values range from 1.71 to 12.66 x 10^{-3} Ω^{-1}, These values are comparable to FOM values of AZO thin films ranging from 10^{-4} to 10^{-2} Ω^{-1} as reported in refs. [5,24,42].

In **Figure 7a**, the AZO40, AZO30 and AZO20 thin films exhibit a lower sheet resistance compared to AZO thin films grown by ALD reported in refs.[12,19,26,30,32,43]. Moreover, it is also worth mentioning that the reported optical transmittance of AZO thin films shown in **Figure 7a** are extracted at different wavelength, or deduced from reported FOM and electrical resistivity values,

which can affect the accuracy of the comparison. For instance, the optical transmittance values of AZO thin films grown by ALD in refs.[26,43] are extracted at 550 nm-wavelength, which is around the maximum peak position of optical transmittance spectra of the AZO films. In our case, the maximum peak position of optical transmittance spectra is located at around 650 nm-wavelength as seen in **Figure 6a**, where the optical transmittance value of the present AZO films can reach up to 99%. The red and blue symbols in **Figure 7a** show that the present AZO thin films compete very well in the field of ALD and can act as a more eco-friendly TCM for nanostructure-based devices in many types of electronic and optoelectronic applications.

In **Figure 7b**, the present thin films exhibit a low sheet resistance and high optical transmittance, which are comparable to those of other AZO films except ITO films whose performance is higher. Although the sheet resistances of the present AZO thin films are slightly higher than those of some AZO films grown by magnetron sputtering, they are still low as compared to AZO films grown by ALD or other techniques. The optical transmittances of the present AZO thin films grown by ALD are instead higher than those of AZO films grown by magnetron sputtering. Furthermore, **Figure 8** illustrates the comparison of FOM values for AZO thin films grown by ALD as reported in refs.[12,19,26,30,32,43] and in this work. The results highlight that the present AZO30 thin film achieves the highest FOM value compared to others.

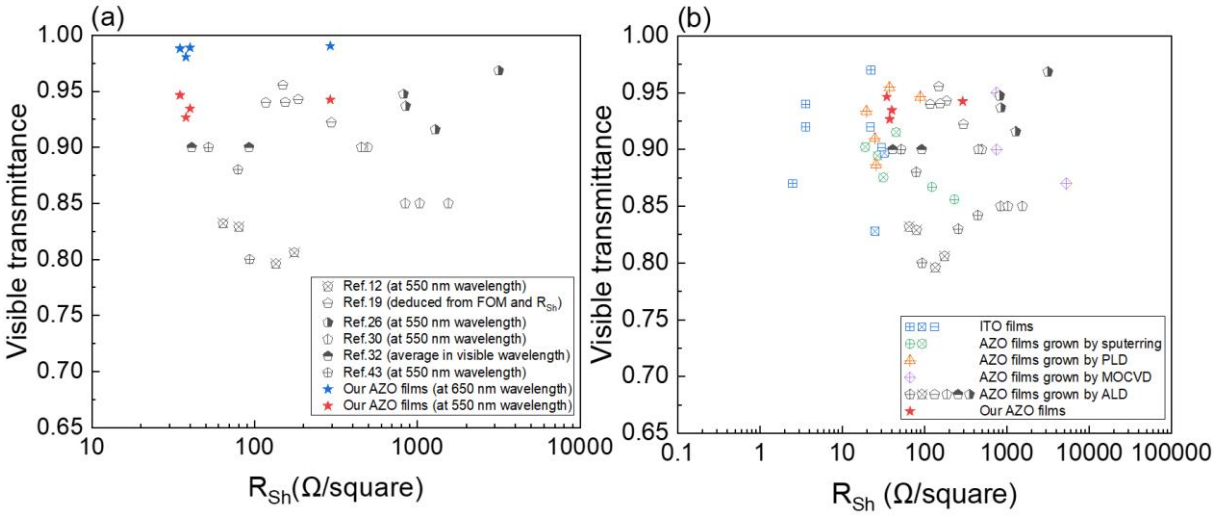

Figure 7: (a) Visible transmittance as a function of the sheet resistance for AZO films grown by ALD. In this graph, the 180 nm-thick AZO films developed in this work is compared with the 200 nm-thick AZO films from ref.[12], 77 nm-thick AZO films from ref.[19], 145 - 253 nm-thick AZO films from ref. [26], 100 nm-thick AZO films from ref.[30], 130 - 200 nm-thick AZO films from ref.[32], and 200 nm-thick AZO films from ref.[43]. (b) Visible transmittance as a function of the sheet resistance for transparent electrodes: ITO films from refs.[42,44,45], AZO films grown by magnetron sputtering from refs.[5,42], by PLD from ref.[16], by sol-gel process from ref.[17], by MOCVD from refs.[18], by ALD from

refs.[12,19,26,30,32,43], and from our work. The presented visible transmittance values exclude the contribution of the substrates.

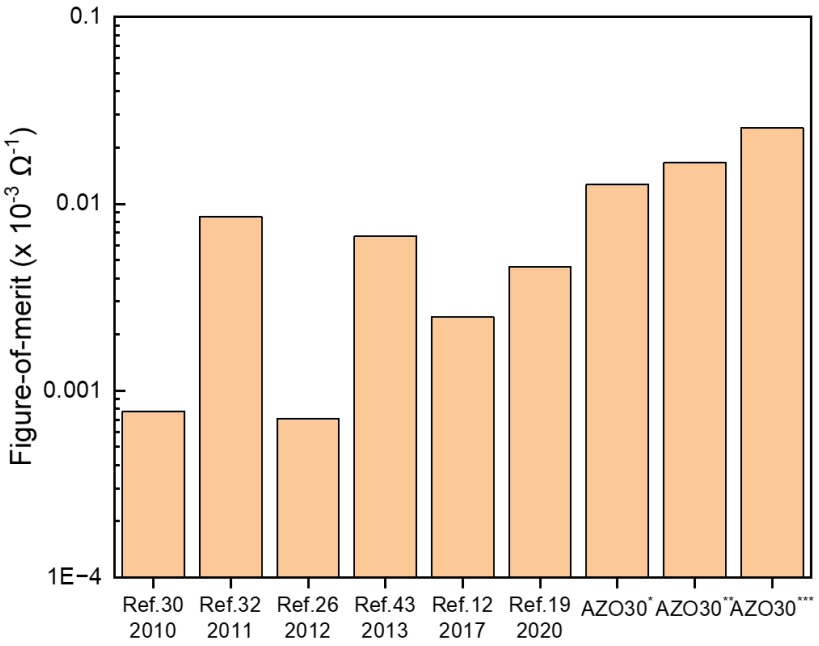

Figure 8: Highest figure-of-merit values of AZO thin films grown by ALD in refs.[12,19,26,30,32,43] and in our work. Figure-of-merit values are calculated based on the mean optical transmittance excluding transmittance of substrates. For our AZO30 thin film, the FOM value is calculated using the average optical transmittance within the 400-700 nm-wavelength range (AZO30*), extracted at 500 nm-wavelength (AZO30**), or extracted at 650 nm-wavelength (AZO30***).

4. Conclusion

In summary, we have demonstrated the possibility to modify the structural orientation of AZO thin films grown by ALD while still achieving a low electrical resistivity and a high visible light transmittance. By changing the cycle ratio of DEZn to TMA, the Al atomic concentration is varied in the range of 0.3 - 6.7%. While the thickness of AZO thin films is kept constant, the resulting morphology strongly depends on the Al atomic concentration. The XRD analysis reveals that the AZO thin film is changed from randomly to highly *c*-axis oriented, and then to partially crystallized structure with the further increase of Al atomic concentration. An excessive Al doping causes a degradation of the crystallinity of AZO thin films due to the large distortion inside the lattice. By using a sufficient amount of Al dopants, not only the structural orientation along the *c*-axis is improved, but the electrical resistivity also decreases thanks to the incorporation of Al dopants acting as shallow donors. At 1.1% Al dopants, the AZO thin film shows a remarkably low electrical resistivity of 6.3 x 10^{-4} Ω·cm, which is comparable with the electrical resistivity of ITO thin films. Moreover, this thin film also possesses a high average visible light transmittance above 85%, leading to a high FOM value

calculated at 6.4 x 10^{-3} Ω^{-1}. All these findings show that this AZO thin film is of high interest as eco-friendly TCMs to be integrated in the process flow of many semiconducting devices in optoelectronics and photovoltaics.

Acknowledgements

This work was supported by the French National Research Agency in the framework of the "Investissements d'avenir" program (ANR-15-IDEX-02) through the project CDP NEED. Q.C.B. held a doctoral fellowship from the project CDP NEED. The authors further acknowledge the support from the CNRS Renatech Network through the "Plateforme Technologique Amont" in a cleanroom environment. This research has also benefited from some of the characterization equipments of the Grenoble INP-CMTC platform and from the facilities and expertise of the OPE)N(RA characterization platform of FMNT (FR 2542, fmnt.fr) supported by CNRS, Grenoble INP and UGA. The authors are further grateful to Isabelle Gelard and Laurent Terrier, LMGP, Grenoble, France, for their assistance in FESEM imaging and UV–Vis-NIR spectrophotometry measurements, respectively.

Declaration of Competing Interest

The authors declare that they have no known competing financial interests or personal relationships that could have appeared to influence the work reported in this paper.

References

[1] K. Ellmer, Past achievements and future challenges in the development of optically transparent electrodes, Nat. Photonics. 6 (2012) 809–817. https://doi.org/10.1038/NPHOTON.2012.282.

[2] K. Kawajiri, K. Tahara, S. Uemiya, Lifecycle assessment of critical material substitution: Indium tin oxide and aluminum zinc oxide in transparent electrodes, Resour. Environ. Sustain. 7 (2022) 100047. https://doi.org/10.1016/j.resenv.2022.100047.

[3] C.H. Lim, J. Han, H. Cho, M. Kang, Studies on the Toxicity and Distribution of Indium Compounds According to Particle Size in Sprague-Dawley Rats, Toxicalogical Reseach. 30 (2014) 55–63.

[4] M.A. Badding, N.R. Fix, M.S. Orandle, M.W. Barger, K.M. Dunnick, K.J. Cummings, S.S. Leonard, Pulmonary toxicity of indium-tin oxide production facility particles in rats, J. Appl. Toxicol. 36 (2015) 618–626. https://doi.org/10.1002/jat.3253.

[5] B. Sarma, D. Barman, B.K. Sarma, AZO (Al:ZnO) thin films with high figure of merit as stable indium free transparent conducting oxide, Appl. Surf. Sci. 479 (2019) 786–795.

[6] A. Tuan, T. Pham, N. Minh, O. Kieu, T. Le, D. Van Hoang, T. Huu, T. Bach, V. Cao, Journal of Science : Advanced Materials and Devices High-mobility sputtered F-doped ZnO films as good-performance transparent-electrode layers, J. Sci. Adv. Mater. Devices. 6 (2021) 446–452. https://doi.org/10.1016/j.jsamd.2021.05.004.

[7] A. Way, J. Luke, A.D. Evans, Z. Li, J.-S. Kim, J.R. Durrant, H.K.H. Lee, W.C. Tsoi, Fluorine doped tin oxide as an alternative of indium tin oxide for bottom electrode of semi-transparent organic photovoltaic devices, AIP Adv. 9 (2019) 085220. https://doi.org/10.1063/1.5104333.

[8] A. Madeira, D.T. Papanastasiou, T. Toupance, L. Servant, D. Bellet, I.A. Goldthorpe, Rapid

synthesis of ultra-long silver nanowires for high performance transparent electrodes, Nanoscale Adv. 2 (2020) 3804. https://doi.org/10.1039/d0na00392a.

[9] K. Rana, J. Singh, J. Ahn, A graphene-based transparent electrode for use in fl exible optoelectronic devices, J. Mater. Chem. C. 2 (2014) 2646. https://doi.org/10.1039/c3tc32264e.

[10] W. Yu, D. Han, J. Dong, Y. Cong, G. Cui, Y. Wang, S. Zhang, AZO Thin Film Transistor Performance Enhancement by Capping an Aluminum Layer, IEEE Trans. Electron Devices. 64 (2017) 2228–2232.

[11] X. Yan, W. Li, A.G. Aberle, S. Venkataraj, Textured AZO for thin-film Si solar cells : Towards understanding the effect of AZO film thickness on the surface texturing properties, Procedia Eng. 139 (2016) 134–139. https://doi.org/10.1016/j.proeng.2015.09.214.

[12] H. Liu, Y. Liu, P. Xiong, P. Chen, H. Li, J. Hou, B. Kang, Y. Duan, Aluminum-Doped Zinc Oxide Transparent Electrode Prepared by Atomic Layer Deposition for Organic Light Emitting Devices, IEEE Trans. Nanotechnol. 16 (2017) 634–638.

[13] M. Hjiri, L. El Mir, S.G. Leonardi, A. Pistone, L. Mavilia, G. Neri, Sensors and Actuators B : Chemical Al-doped ZnO for highly sensitive CO gas sensors, Sensors Actuators B. Chem. 196 (2014) 413–420. https://doi.org/10.1016/j.snb.2014.01.068.

[14] C. Justeau, T.S. Tlemcani, G. Poulin-vittrant, K. Nadaud, D. Alquier, A Comparative Study on the Effects of Au, ZnO and AZO Seed Layers on the Performance of ZnO, Materials (Basel). 12 (2019) 2511.

[15] S.-Y. Pung, K.-L. Choy, X. Hou, C. Shan, Preferential growth of ZnO thin films by the atomic layer deposition technique, Nanotechnology. 19 (2008) 435609. https://doi.org/10.1088/0957-4484/19/43/435609.

[16] S. Park, T. Ikegami, K. Ebihara, Investigation of Transparent Conductive Oxide Al-Doped ZnO Films Produced by Pulsed Laser Deposition, Jpn. J. Appl. Phys. 44 (2005) 8027–8031. https://doi.org/10.1143/JJAP.44.8027.

[17] K.N. Tonny, R. Rafique, A. Sharmin, M.S. Bashar, Z.H. Mahmood, Electrical, optical and structural properties of transparent conducting Al doped ZnO (AZO) deposited by sol-gel spin coating, AIP Adv. 8 (2018). https://doi.org/10.1063/1.5023020.

[18] S.A. Ayinde, O. Fasakin, B. Olofinjana, A. V Adedeji, P.O. Oyedare, M.A. Eleruja, E.O.B. Ajayi, Optical, Structural and Electrical Properties of Aluminum Doped Zinc Oxide Thin Films by MOCVD Technique, J. Electron. Mater. 48 (2019) 3655–3661. https://doi.org/10.1007/s11664-019-07123-8.

[19] Y. Wu, F. Cao, X. Ji, Optical and electrical properties of Al-doped ZnO thin films by atomic layer deposition, J. Mater. Sci. Mater. Electron. 31 (2020) 17365–17374. https://doi.org/10.1007/s10854-020-04292-9.

[20] Y. Geng, L. Guo, S. Xu, Q. Sun, S. Ding, H. Lu, D.W. Zhang, Influence of Al Doping on the Properties of ZnO Thin Films Grown by Atomic Layer Deposition, J. Phys. Chem. C. 115 (2011) 12317–12321.

[21] N.P. Dasgupta, S. Neubert, W. Lee, O. Trejo, J. Lee, F.B. Prinz, Atomic Layer Deposition of Al-doped ZnO Films : Effect of Grain Orientation on Conductivity, Chem. Mater. 22 (2010) 4769–4775. https://doi.org/10.1021/cm101227h.

[22] J.Y. Kim, Y.-J. Choi, H.-H. Park, S. Golledge, D.C. Johnson, Effective atomic layer deposition procedure for Al-dopant distribution in ZnO thin films, J. Vac. Sci. Technol. A. 28 (2010) 1111. https://doi.org/10.1116/1.3460905.

[23] B. Joseph, P.K. Manoj, V.K. Vaidyan, Studies on the structural , electrical and optical

properties of Al-doped ZnO thin films prepared by chemical spray deposition, Ceram. Int. 32 (2006) 487–493. https://doi.org/10.1016/j.ceramint.2005.03.029.

[24] J. Jeong, H. Shin, K. Choi, H. Kim, Flexible Al-doped ZnO films grown on PET substrates using linear facing target sputtering for flexible OLEDs, J. Phys. D. Appl. Phys. 43 (2010) 465403. https://doi.org/10.1088/0022-3727/43/46/465403.

[25] S.K. Park, Y.E. Lee, Controlling preferred orientation of ZnO thin films by atomic layer deposition, J. Mater. Sci. 39 (2004) 2195–2197.

[26] T. Dhakal, D. Vanhart, R. Christian, A. Nandur, A. Sharma, C.R. Westgate, Growth morphology and electrical/optical properties of Al-doped ZnO thin films grown by atomic layer deposition films grown by atomic layer deposition, J. Vac. Sci. Technol. A. 30 (2012) 021202.

[27] Q.C. Bui, G. Ardila, H. Roussel, C. Jimenez, I. Gelard, O. Chaix-pluchery, X. Mescot, S. Boubenia, B. Salem, V. Consonni, Tuneable polarity and enhanced piezoelectric response of ZnO thin films grown by metal – organic chemical vapour deposition, Mater. Adv. 3 (2022) 498–513. https://doi.org/10.1039/d1ma00921d.

[28] A. van der DRIFT, Evolutionary selection, a principle governing growth orientation in vapour-deposited layers, Philips Res. Reports. 22 (1967) 267–288.

[29] A. Wander, F. Schedin, P. Steadman, A. Norris, R. Mcgrath, T.S. Turner, G. Thornton, N.M. Harrison, Stability of Polar Oxide Surfaces, Phys. Rev. Lett. 86 (2001) 3811. https://doi.org/10.1103/PhysRevLett.86.3811.

[30] P. Banerjee, W.-J. Lee, K.-R. Bae, S.B. Lee, G.W. Rubloff, Structural, electrical, and optical properties of atomic layer deposition Al-doped ZnO films, J. Appl. Phys. 108 (2010) 043504. https://doi.org/10.1063/1.3466987.

[31] G. Luka, L. Wachnicki, B.S. Witkowski, T.A. Krajewski, R. Jakiela, E. Guziewicz, M. Godlewski, The uniformity of Al distribution in aluminum-doped zinc oxide films grown by atomic layer deposition, Mater. Sci. Eng. B. 176 (2011) 237–241. https://doi.org/10.1016/j.mseb.2010.11.014.

[32] G. Luka, T.A. Krajewski, B.S. Witkowski, G. Wisz, I.S. Virt, E. Guziewicz, M. Godlewski, Aluminum-doped zinc oxide films grown by atomic layer deposition for transparent electrode applications, J. Mater. Sci. Mater. Electron. 22 (2011) 1810–1815. https://doi.org/10.1007/s10854-011-0367-0.

[33] Q.C. Bui, G. Ardila, E. Sarigiannidou, H. Roussel, C. Jiménez, O. Chaix-Pluchery, Y. Guerfi, F. Bassani, F. Donatini, X. Mescot, B. Salem, V. Consonni, Morphology Transition of ZnO from Thin Film to Nanowires on Silicon and its Correlated Enhanced Zinc Polarity Uniformity and Piezoelectric Responses, ACS Appl. Mater. Interfaces. 12 (2020) 29583–29593. https://doi.org/10.1021/acsami.0c04112.

[34] Q.C. Bui, B. Salem, H. Roussel, X. Mescot, Y. Guerfi, C. Jiménez, V. Consonni, G. Ardila, Effects of thermal annealing on the structural and electrical properties of ZnO thin films for boosting their piezoelectric response, J. Alloys Compd. 870 (2021) 159512. https://doi.org/10.1016/j.jallcom.2021.159512.

[35] V.H. Nguyen, J. Resende, C. Jiménez, J.-L. Deschanvres, P. Carroy, D. Muñoz, D. Bellet, D. Muñoz-Rojas, Deposition of ZnO based thin films by atmospheric pressure spatial atomic layer deposition for application in solar cells, J. Renew. Sustain. Energy. 9 (2017) 021203. https://doi.org/10.1063/1.4979822.

[36] A. Seweryn, R. Pietruszka, B.S. Witkowski, A. Wierzbicka, R. Jakiela, P. Sybilski, M. Godlewski, Structural and Electrical Parameters of ZnO Thin Films Grown by ALD with either Water or Ozone as Oxygen Precursor, Cryst. 2019. 9 (2019) 554.

[37] S. Mishra, E. Przezdziecka, W. Wozniak, A. Adhikari, R. Jakiela, W. Paszkowicz, A. Sulich, M. Ozga, K. Kopalko, E. Guziewicz, Structural Properties of Thin ZnO Films Deposited by ALD under O-Rich and Zn-Rich Growth Conditions and Their, Materials (Basel). 14 (2021) 4048.

[38] B. Xia, J.J. Ganem, E. Briand, S. Steydli, H. Tancrez, I. Vickridge, The carbon and hydrogen contents in ALD-grown ZnO films define a narrow ALD temperature window, Vacuum. 190 (2021) 110289. https://doi.org/10.1016/j.vacuum.2021.110289.

[39] T. Cossuet, F. Donatini, A.M. Lord, E. Appert, J. Pernot, V. Consonni, Polarity-Dependent High Electrical Conductivity of ZnO Nanorods and Its Relation to Hydrogen, J. Phys. Chem. C. 122 (2018) 22767–22775. https://doi.org/10.1021/acs.jpcc.8b07388.

[40] A. Wang, T. Chen, S. Lu, Z. Wu, Y. Li, H. Chen, Y. Wang, Effects of doping and annealing on properties of ZnO films grown by atomic layer deposition, Nanoscale Res. Lett. 10 (2015) 75. https://doi.org/10.1186/s11671-015-0801-y.

[41] S. Lin, J. Huang, P. Sajgalik, The properties of heavily Al-doped ZnO films before and after annealing in the different atmosphere, Surf. Coat. Technol. 185 (2004) 254–263. https://doi.org/10.1016/j.surfcoat.2003.12.007.

[42] R.A. Mereu, S. Marchionna, A. Le Donne, L. Ciontea, S. Binetti, M. Acciarri, Optical and electrical studies of transparent conductive AZO and ITO sputtered thin films for CIGS photovoltaics, Phys. Status Solidi C. 11 (2014) 1464–1467. https://doi.org/10.1002/pssc.201300631.

[43] S.C. Gong, Y.-J. Choi, H. Kim, C.-S. Park, H.-H. Park, J.G. Jang, H.J. Chang, G.Y. Yeom, Aluminum-doped zinc oxide formed by atomic layer deposition for use as anodes in organic light emitting diodes, J. Vac. Sci. Technol. A. 31 (2013) 01A101. https://doi.org/10.1116/1.4738749.

[44] Z. Chen, W. Li, R. Li, Y. Zhang, G. Xu, H. Cheng, Fabrication of Highly Transparent and Conductive Indium − Tin Oxide Thin Films with a High Figure of Merit via Solution Processing, Langmuir. 29 (2013) 13836−13842.

[45] A. Khrypunova, D. Kudii, I. Khrypunova, The Optical and Electrical Properties ITO Thin Film, 2018 IEEE 3rd Int. Conf. Intell. Energy Power Syst. (2018) 229–234.